Diffraction catastrophes and semiclassical quantum mechanics for Veselago lensing in graphene

K. J. A. Reijnders* and M. I. Katsnelson
Radboud University, Institute for Molecules and Materials, Heyendaalseweg 135, 6525 AJ Nijmegen, The Netherlands
(Received 7 April 2017; published 24 July 2017)

We study the effect of trigonal warping on the focusing of electrons by *n-p* junctions in graphene. We find that perfect focusing, which was predicted for massless Dirac fermions, is only preserved for one specific lattice orientation. In the general case, trigonal warping leads to the formation of cusp caustics, with a different position of the focus for graphene's two valleys. We develop a semiclassical theory to compute these positions and find very good agreement with tight-binding simulations. Considering the transmission as a function of potential strength, we find that trigonal warping splits the single Dirac peak into two distinct peaks, leading to valley polarization. We obtain the transmission curves from tight-binding simulations and find that they are in very good agreement with the results of a billiard model that incorporates trigonal warping. Furthermore, the positions of the transmission maxima and the scaling of the peak width are accurately predicted by our semiclassical theory. Our semiclassical analysis can easily be carried over to other Dirac materials, which generally have different Fermi surface distortions.

DOI: 10.1103/PhysRevB.96.045305

Veselago lenses [1] are special types of lenses, made of materials with a negative refractive index. Such lenses can overcome the diffraction limit [2] and can nowadays be realized in metamaterials [3–5], chiral metamaterials [6–9], and photonic crystals [10,11]. An electronic analog of a Veselago lens can be created using *n-p* junctions, with the classical trajectories of the charge carriers playing the role of the rays in geometrical optics. Such junctions focus electrons, because the group velocity for holes is in the direction opposite to their phase velocity, whereas the two velocities are in the same direction for electrons. However, in conventional semiconductors, such interfaces are unsuitable because of their high reflectivity, owing to the presence of a depletion region.

Cheianov *et al.* [12] realized that graphene does not have this drawback. It has zero band gap, as the valence and conduction bands touch at two nonequivalent corners of the Brillouin zone, known as K and K'. The low-energy charge carriers are ballistic over large distances and follow the Dirac equation [13–18]. This gives rise to Klein tunneling: normally incident electrons are transmitted with unit probability [19–27], which makes the interface exceptionally transparent. Recently, Veselago lensing in graphene was experimentally observed [27,28]. Furthermore, a two-dimensional Dirac fermion microscope based on Veselago lensing was proposed [29].

Theoretical studies have used the Dirac equation to investigate focusing by flat [12,30] and circular [31–33] junctions and in zigzag nanoribbons [34]. It was shown that when the electron and hole charge carrier densities are equal, a flat interface is able to focus all trajectories into a single point [12]. According to catastrophe theory [35–38], such a situation is exceptional: any perturbation of the Hamiltonian will ruin this ideal focus. Indeed, in tight-binding simulations of an *n-p* junction [39], where transmission was studied as a function of potential strength, a direction-dependent broadening of the transmission peak was observed. However, the precise origin of this broadening was not clarified.

An important correction to the Dirac Hamiltonian is the second-order term in the expansion of graphene's tight-binding Hamiltonian, known as the trigonal warping term [18,40,41]. When adding this term, the Hamiltonian becomes dependent on the crystallographic direction of the lattice and becomes different for the two valleys, leading to different classical trajectories. Using this principle, a valley beam splitter based on an n-p-n' junction was devised [42], in which the trajectories in the K and K' valleys are deflected in different angular directions. Creating valley polarization [43–47] is important for graphene valleytronics applications, where the valley index is used to encode information in a way similar to spintronics.

In this paper, we develop a complete semiclassical theory of Veselago lensing by an *n-p* junction in the presence of trigonal warping. We show that the ideal focus generally disappears and analyze the different diffraction catastrophes, known as caustics [35–38], that are formed. We show that electrons from the K and K' valleys are generally focused at different positions, even at moderate energies. We obtain these positions using semiclassical methods [30,48,49] based on the Pearcey function [50–52] and find very good agreement with tight-binding simulations using the Kwant code [53]. We also show that an initial sublattice polarization leads to tilting of the focus. Furthermore, we obtain the transmission as a function of the hole carrier density from both tight-binding simulations [53] and a semiclassical billiard model [54,55] that incorporates trigonal warping. We find that trigonal warping explains the previously observed peak broadening [39] and that our semiclassical theory accurately predicts the positions of the transmission maxima and the scaling of the peak widths. Since the transmission maximum occurs at a different potential for the two valleys, we find that a graphene *n-p* junction can act as a valley filter and that one can manipulate the polarization by changing the potential strength. This is similar to the situation in chiral metamaterials [6–9], where one can select a certain polarization by tuning the frequency of the incident light.

Trigonal warping adds terms that are quadratic in momentum to the linear term in the massless Dirac Hamiltonian [18,40,41]. We make all terms in the Hamiltonian

*K.Reijnders@science.ru.nl

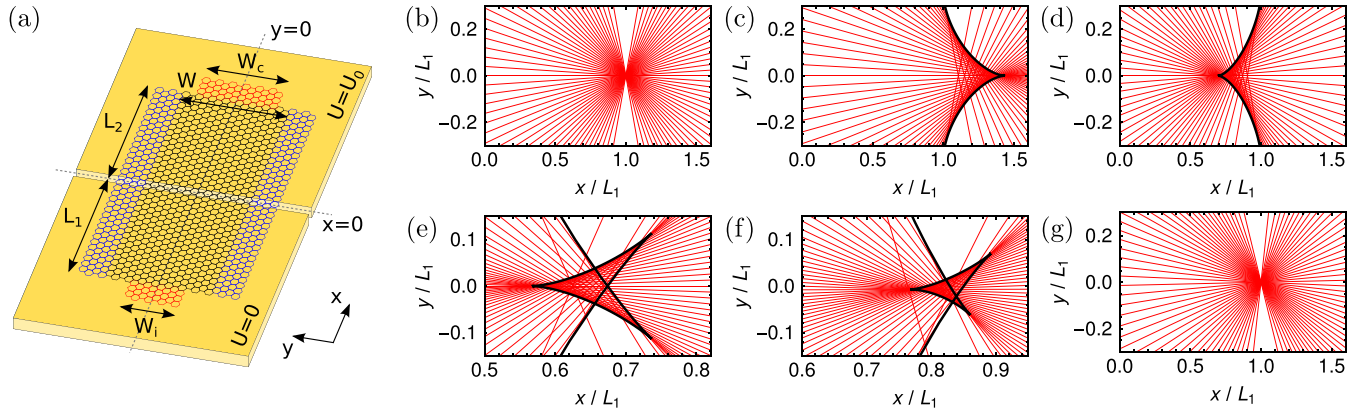

FIG. 1. (a) Simulation setup with an injector and collector lead (red) and drain leads on each side (blue). (b) Classical trajectories for the massless Dirac Hamiltonian at $U_0 = 2E$. (c)–(g) Classical trajectories (red) and caustics (black) for the Hamiltonian including trigonal warping. Unless otherwise indicated, $E = 0.4$ eV. (c) K valley, $U_0 = 0.8$ eV, $\theta = 0$; (d) K' valley, $U_0 = 0.8$ eV, $\theta = 0$; (e) section of the butterfly caustic. K' valley, $E = 0.6$ eV, $U_0 = 1.18$ eV, $\theta = 0$; (f) K' valley, $U_0 = 0.795$ eV, $\theta = \pi/12$; (g) $U_0 = 0.8$ eV, $\theta = \pi/6$.

dimensionless [24] by scaling energies with the electron energy E and lengths with L_1, the distance from the source to the junction; see Fig. 1(a). Using first-order perturbation theory, we obtain the classical Hamiltonian in dimensionless variables [18,40,41,56,57]:

$$H_\alpha^\pm = \pm(|\mathbf{p}| + \alpha\mu|\mathbf{p}|^2 \cos[3(\phi_\mathbf{p} + \theta)]) + U(\mathbf{x}), \qquad (1)$$

where $\mu = E/6t$, with t the nearest-neighbor hopping, indicates the relative importance of the quadratic term and α equals $+1$ (-1) for valley K' (K). Furthermore, $\phi_\mathbf{p} = \arctan(p_y/p_x)$ and the angle θ determines the orientation of the lattice, with $\theta = 0$ corresponding to zigzag edges along the x direction. The dimensionless semiclassical parameter h equals $3ta_{CC}/2EL_1$, with a_{CC} the carbon-carbon distance.

We consider a sharp, one-dimensional junction: $U(\mathbf{x}) = U_0\Theta(x)$, with $\Theta(x)$ the Heaviside step function. Then p_y is conserved and the classical action for an electron with energy E emitted from $(-L_1,0)$ equals [12,30]

$$S_{np}(x, y, p_y) = L_1\, p_{x,e,\alpha}(p_y) + x\, p_{x,h,\alpha}(p_y) + y\, p_y, \qquad (2)$$

with $p_{x,e,\alpha}$ $(p_{x,h,\alpha})$ the longitudinal momentum in electron (hole) region, i.e., $H_\alpha^+(p_{x,e,\alpha}(p_y), p_y) = E$. The classical trajectories, i.e., the points where $\partial S_{np}/\partial p_y = 0$, and the caustics, where $\partial^2 S_{np}/\partial p_y^2$ vanishes as well, are plotted in Fig. 1 for various parameters. The Dirac Hamiltonian, $\mu = 0$ in Eq. (1) is symmetric in p_x and p_y. When $U_0 = 2E$, this leads to an ideal focus [12], at which all derivatives of S_{np} with respect to p_y vanish [30]. This generally changes when we include trigonal warping. For $\theta = 0$, the symmetry in p_y is preserved, leading to reflection symmetry in the x axis. However, the symmetry in p_x is broken and we obtain cusp caustics, shown in Figs. 1(c) and 1(d). Because we also break the symmetry

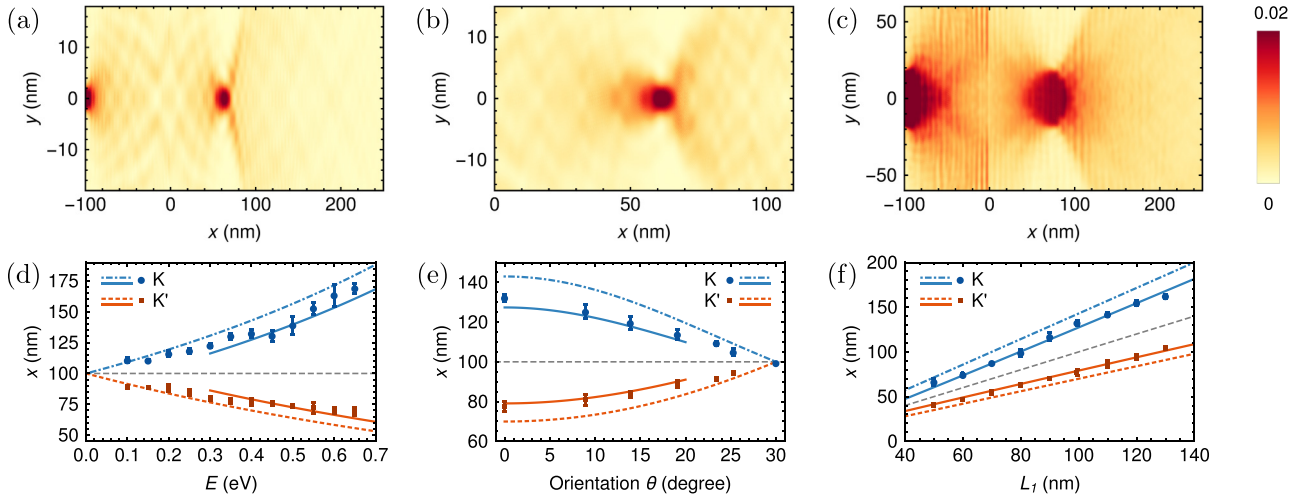

FIG. 2. (a)–(c) Results of the tight-binding simulations with $L_1 = 100$ nm. The density $|\Psi_{\mathrm{av},\alpha}|^2$ is averaged over sublattices and summed over lead modes in valley α. (a) K' valley, $E = 0.6$ eV, $U_0 = 2E$, $W_i = 7.5$ nm; (b) K' valley, $E = 0.6$ eV, $U_0 = 1.18$ eV, $W_i = 7.5$ nm; cf. the classical trajectories in Fig. 1(e); (c) K' valley, $E = 0.4$ eV, $U_0 = 2E$, $W_i = 40$ nm. (d)–(f) Position, on the x axis, of the caustic (dashed and dashed-dotted lines), semiclassical maximum (solid lines), and simulated maximum (symbols) for varying energy E, lattice orientation θ, and L_1. The dashed gray lines indicate the Dirac result. The parameters equal (e),(f) $E = 0.4$ eV, (d),(f) $\theta = 0$, (d),(e) $L_1 = 100$ nm, (d),(f) $W_i = 40$ nm, and (e) $W_i = 50$ nm. In all cases $U_0 = 2E$.

between the valleys K and K', their cusp points, at which $\partial^4 S_{np}/\partial p_y^4 \neq 0$, are at different positions on the x axis. Tuning the potential, we obtain sections of the butterfly caustic, see Fig. 1(e), and eventually pass through the butterfly singularity, at which $\partial^4 S_{np}/\partial p_y^4 = 0$, but $\partial^6 S_{np}/\partial p_y^6 \neq 0$ [30,36]. For generic θ, Fig. 1(f), both symmetries are broken and the cusp point is no longer on the x axis. Only when $\theta = \pi/6$ (armchair edges), the symmetry in p_x is restored and we recover an ideal focus at $U_0 = 2E$; see Fig. 1(g).

From here on, we consider zigzag edges along the x direction ($\theta = 0$), unless otherwise indicated, as they illustrate the generic situation. We obtain an expression for $x_{\mathrm{cusp},\alpha}$ by solving $\partial^2 S_{np}/\partial p_y^2 = 0$ for x, and setting $p_y = 0$ [30]. Expanding the result up to second order in $\alpha\mu$, we find, in units with dimensions,

$$x_{\mathrm{cusp},\alpha} = L_1 \frac{U_0 - E}{E}\left(1 - \alpha\frac{4U_0}{3t}\right) \overset{U_0=2E}{=\!=} L_1 - \frac{8\alpha E}{3t}L_1. \quad (3)$$

Hence the cusp point for the valley K (K') is always to the right (left) of the focus for the Dirac Hamiltonian, given by the first term. Although the above expansion is only sufficient for low energies, it clearly indicates that the effect is sizable.

We study these effects by performing tight-binding simulations with Kwant [53]. We use the setup of Ref. [39], shown in Fig. 1(a), where current enters the sample through an injector lead and is able to exit through a collector lead and through drain leads on each side (see Supplemental Material [58]). Considering large L_2 and $W_c = W$, we compute the sample wave function. Figures 2(a)–2(c) show the resulting density, averaged over sublattices and summed over lead modes [30,59]. For narrow leads, i.e., large $h_{\mathrm{lead}} = \hbar v_F/EW_i$, we observe cusp caustics in the valleys K and K'; see Fig. 2(a). By adjusting E and U_0, we also observe sections of the butterfly caustic; see Fig. 2(b). Figure 2(c) shows that we obtain a bright focusing spot for wide leads (small h_{lead}), as predicted in Ref. [30]. Subsequently, we fit a Gaussian to a subset of the points on the x axis. Averaging over subsets, we obtain the position of the maximum and an error estimate.

Within the semiclassical approximation, the wave function near a cusp can be constructed in terms of the Pearcey function [30,48,49,58]. We find the parameters for this function by expanding the action (2) up to fourth order in p_y. Figures 2(d)–2(f) show the predictions $x_{\mathrm{max},\alpha}$, obtained from maximizing this wave function, as a function of electron energy, lattice orientation, and L_1. They are in very good agreement with the positions extracted from the simulations. Note that the approximation fails for low energies, or near $\theta = \pi/6$, as we are too close to the ideal focus, at which $\partial^4 S_{np}/\partial p_y^4 = 0$. However, in these cases, $x_{\mathrm{cusp},\alpha}$ provides a good estimate.

Experimentally, one typically measures the transmission T as a function of potential strength. We therefore fix L_1 and L_2, set $W_c = W_i$, and compute the intravalley scattering for varying U_0 using Kwant. We compare these results with a semiclassical billiard model [54,55] that incorporates trigonal warping in the trajectories and has uniformly distributed initial positions and transversal momenta. Figure 3 shows that the agreement between the two methods is very good. Note that the tight-binding transmission is slightly higher than the billiard result on the right (left) of the peak for valley K (K'), most likely because of interference. Higher order effects and intervalley scattering only mildly influence the results. Figure 3(e) shows that, for small h_{lead}, passing through the butterfly singularity does not significantly enhance the transmission.

Valley splitting is observed at all simulated energies and the total transmission peak is broadened with respect to the result of a Dirac billiard model, which explains earlier observations [39]. The transmission maximum for the K valley is always at a lower potential. Setting $x_{\mathrm{cusp},\alpha} = L_2$ in Eq. (3) and solving for U_0, we obtain, up to $O(\mu^2)$, in units with dimensions,

$$U_{0,\mathrm{cusp},\alpha} = E\frac{L_1 + L_2}{L_1}\left(1 + \alpha\frac{4E}{3t}\frac{L_2}{L_1}\right) \overset{L_1=L_2}{=\!=} 2E + \frac{8\alpha E^2}{3t}. \quad (4)$$

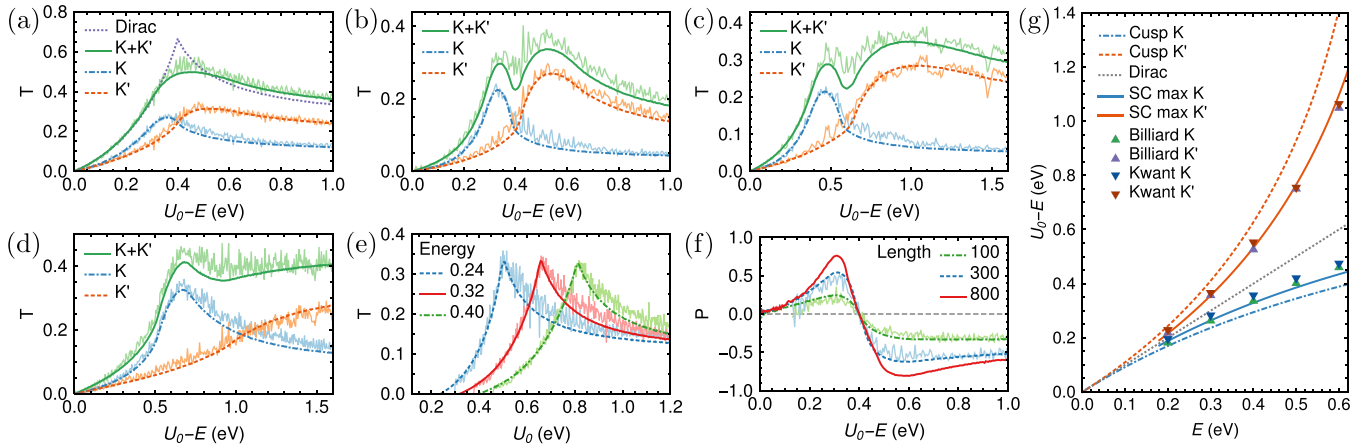

FIG. 3. (a)–(e) Intravalley transmission as a function of potential strength obtained from Kwant (light colors, wavy lines) and a billiard model (darker colors, smooth lines). (a) $E = 0.4$ eV, $L_1 = L_2 = 100$ nm; (b) $E = 0.4$ eV, $L_1 = L_2 = 300$ nm; (c) $E = 0.6$ eV, $L_1 = L_2 = 200$ nm; (d) $E = 0.4$ eV, $L_1 = 100$ nm, $L_2 = 300$ nm. (e) K valley, $L_1 = 100$ nm, $L_2 = 140$ nm for various energies (in eV). For $E = 0.24$ eV, $\partial^4 S_{np}/\partial p_y^4$ vanishes at $U_0 = 0.5$ eV and $x = L_2$. (f) Valley polarization $P = (T_K - T_{K'})/(T_K + T_{K'})$ as a function of potential for $E = 0.4$ eV and various $L_1 = L_2$ (in nm). (g) Maximum of the simulated intensity as a function of energy for $L_1 = L_2 = 200$ nm. We also plot the potentials at which $x_{\mathrm{cusp},\alpha}$ and the semiclassical (SC) $x_{\mathrm{max},\alpha}$ equal L_2. For all figures $W_i = W_c = 50$ nm.

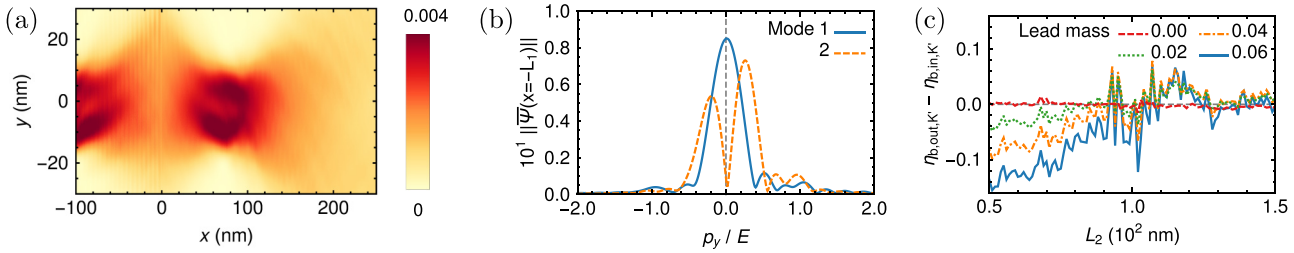

FIG. 4. (a) Density $|\Psi_{\mathrm{av},K'}|^2$ from tight-binding simulations for $E = 0.4$ eV, $m_{\mathrm{lead}} = 0.375$ eV, and $W_i = 40$ nm. (b) Fourier transform (for each lead mode) of the wave function from (a) at $x = -L_1$. (c) Symmetry breaking as a function of L_2 for various m_{lead} (in eV). K' valley, $E = 0.1$ eV, $W_i = 50$ nm. For all figures $L_1 = 100$ nm and $U_0 = 2E$.

We also obtain predictions $U_{0,\mathrm{max},\alpha}$ for the positions of the maxima from our semiclassical theory. Solving $x_{\mathrm{max},\alpha} = L_2$, we obtain values that are in excellent agreement with the simulated peak positions; see Fig. 3(g). As $\partial^4 S_{np}/\partial p_y^4$ is lower at the K peak, our theory also correctly predicts that it has lower maximal transmission.

The valley polarization can be increased by going to higher energies, which increases the peak splitting. Alternatively, one can increase L_2; see Fig. 3(d). Finally, one can also increase both L_1 and L_2, see Fig. 3(f), which decreases the peak width ΔU_0. We obtain a semiclassical prediction for the scaling behavior of ΔU_0 by performing a Taylor expansion of the equation $x_{\mathrm{max},\alpha} = L_2$ around $U_{0,\mathrm{cusp},\alpha}$. For $L_1 = L_2 = L$, we find that $\Delta U_0 \propto L^{-1/2}$ in leading order, which is in perfect agreement with the billiard results.

Finally, we briefly discuss symmetry breaking due to an initial sublattice polarization [30]. When we add a constant mass m_{lead} in the lead, we observe tilting of the main focus; see Fig. 4. Inspecting the Fourier transform, we observe that it is not symmetric in p_y, verifying earlier predictions [30]. To certify that this effect can be attributed to the Dirac character of the electrons, and not to trigonal warping, we extract the wave function at $x = -L_1$ from Kwant and compute its evolution using the continuum Dirac equations [30]. This reproduces the tilting, but changes the position of the focus, confirming our hypothesis.

The symmetry breaking can be quantified by setting $W_c = W$ and subsequently splitting the collector lead at $y = 0$. We then extract the relative transmission $\eta_{b,\mathrm{out},\alpha}$ through the bottom ($y < 0$) collector lead and subtract the relative intensity $\eta_{b,\mathrm{in},\alpha}$ located on the sites with negative y for the incoming modes. Figure 4(c) shows that the amount of symmetry breaking strongly depends on L_2, as expected for a tilted focus. In agreement with predictions made for the Green's function [30], it increases with increasing mass, decreases with increasing energy, and changes sign when we change the sign of the mass. Simulating transmission as a function of potential strength, initial polarization seems to slightly decrease the valley polarization.

In short, we have developed a complete semiclassical theory of Veselago lensing in the presence of trigonal warping. We have observed both cusp and butterfly singularities, which provide an interesting relation between the physics of graphene and catastrophe theory [35–38]. Our theory is in excellent agreement with tight-binding simulations and shows that the system generally exhibits valley polarization. We believe that our predictions could be experimentally verified, using, for instance, a transverse magnetic focusing setup [27]. Although this would require rather high energies, these have been experimentally realized [60–63]. We remark that a smooth junction will lead to additional peak broadening [27,39,64], but this makes a theoretical study much more complicated [24].

We emphasize that our analysis of the disintegration of the ideal focus does not fundamentally depend on the fact that the Fermi surface distortion is trigonal: any distortion that breaks the symmetry in p_x will lead to the formation of cusp caustics. Therefore, our semiclassical analysis can easily be carried over to other Dirac materials, such as topological insulators [65,66]. Deviations from Dirac behavior may for instance be important for the proposed application of Weyl semimetals in scanning tunneling microscopes [67]. Since other Dirac materials generally exhibit stronger band bending than graphene, the deviations from the Dirac behavior will be much stronger and therefore visible at lower energies.

We are grateful to Misha Titov and Erik van Loon for helpful discussions. The authors acknowledge support from the European Research Council (ERC) Advanced Grant No. 338957 FEMTO/NANO and from the Netherlands Organisation for Scientific Research (NWO) via the Spinoza Prize.

[1] V. G. Veselago, Sov. Phys. Usp. **10**, 509 (1968).
[2] J. B. Pendry, Phys. Rev. Lett. **85**, 3966 (2000).
[3] D. R. Smith, W. J. Padilla, D. C. Vier, S. C. Nemat-Nasser, and S. Schultz, Phys. Rev. Lett. **84**, 4184 (2000).
[4] A. A. Houck, J. B. Brock, and I. L. Chuang, Phys. Rev. Lett. **90**, 137401 (2003).
[5] A. Grbic and G. V. Eleftheriades, Phys. Rev. Lett. **92**, 117403 (2004).
[6] S. Tretyakov, I. Nefedov, A. Sihvola, S. Maslovski, and C. Simovski, J. Electromagn. Waves. Appl. **17**, 695 (2003).
[7] J. B. Pendry, Science **306**, 1353 (2004).
[8] S. Zhang, Y.-S. Park, J. Li, X. Lu, W. Zhang, and X. Zhang, Phys. Rev. Lett. **102**, 023901 (2009).
[9] X. Xiong, W.-H. Sun, Y.-J. Bao, M. Wang, R.-W. Peng, C. Sun, X. Lu, J. Shao, Z.-F. Li, and N.-B. Ming, Phys. Rev. B **81**, 075119 (2010).

[10] P. V. Parimi, W. T. Lu, P. Vodo, J. Sokoloff, J. S. Derov, and S. Sridhar, Phys. Rev. Lett. **92**, 127401 (2004).
[11] E. Cubukcu, K. Aydin, E. Ozbay, S. Foteinopoulou, and C. M. Soukoulis, Phys. Rev. Lett. **91**, 207401 (2003).
[12] V. V. Cheianov, V. Fal'ko, and B. L. Altshuler, Science **315**, 1252 (2007).
[13] P. R. Wallace, Phys. Rev. **71**, 622 (1947).
[14] J. W. McClure, Phys. Rev. **104**, 666 (1956).
[15] J. C. Slonczewski and P. R. Weiss, Phys. Rev. **109**, 272 (1958).
[16] G. W. Semenoff, Phys. Rev. Lett. **53**, 2449 (1984).
[17] A. H. Castro Neto, F. Guinea, N. M. R. Peres, K. S. Novoselov, and A. K. Geim, Rev. Mod. Phys **81**, 109 (2009).
[18] M. I. Katsnelson, *Graphene: Carbon in Two Dimensions* (Cambridge University Press, Cambridge, UK, 2013).
[19] O. Klein, Z. Phys. **53**, 157 (1929).
[20] M. I. Katsnelson, K. S. Novoselov, and A. K. Geim, Nat. Phys. **2**, 620 (2006).
[21] V. V. Cheianov and V. I. Fal'ko, Phys. Rev. B **74**, 041403 (2006).
[22] A. V. Shytov, M. S. Rudner, and L. S. Levitov, Phys. Rev. Lett. **101**, 156804 (2008).
[23] T. Tudorovskiy, K. J. A. Reijnders, and M. I. Katsnelson, Phys. Scr. **T146**, 014010 (2012).
[24] K. J. A. Reijnders, T. Tudorovskiy, and M. I. Katsnelson, Ann. Phys. (NY) **333**, 155 (2013).
[25] A. F. Young and P. Kim, Nat. Phys. **5**, 222 (2009).
[26] N. Stander, B. Huard, and D. Goldhaber-Gordon, Phys. Rev. Lett. **102**, 026807 (2009).
[27] S. Chen, Z. Han, M. M. Elahi, K. M. M. Habib, L. Wang, B. Wen, Y. Gao, T. Taniguchi, K. Watanabe, J. Hone *et al.*, Science **353**, 1522 (2016).
[28] G.-H. Lee, G.-H. Park, and H.-J. Lee, Nat. Phys. **11**, 925 (2015).
[29] P. Bøggild, J. M. Caridad, C. Stampfer, G. Calogero, N. R. Papior, and M. Brandbyge, Nat. Commun. **8**, 15783 (2017).
[30] K. J. A. Reijnders and M. I. Katsnelson, Phys. Rev. B **95**, 115310 (2017).
[31] J. Cserti, A. Pályi, and C. Péterfalvi, Phys. Rev. Lett. **99**, 246801 (2007).
[32] C. Péterfalvi, A. Pályi, Á. Rusznyák, J. Koltai, and J. Cserti, Physica Status Solidi B **247**, 2949 (2010).
[33] J.-S. Wu and M. M. Fogler, Phys. Rev. B **90**, 235402 (2014).
[34] S.-J. Choi, S. Park, and H.-S. Sim, Phys. Rev. B **89**, 155412 (2014).
[35] M. V. Berry and C. Upstill, in *Progress in Optics XVIII*, edited by E. Wolf (North-Holland, Amsterdam, 1980).
[36] T. Poston and I. N. Stewart, *Catastrophe Theory and Its Applications* (Pitman, Boston, 1978).
[37] V. I. Arnold, S. M. Gusein-Zade, and A. N. Varchenko, *Singularities of Differentiable Maps* (Birkhäuser, Basel, 1982), Vol. 1.
[38] V. I. Arnold, Russ. Math. Surv. **30**, 1 (1975).
[39] S. P. Milovanović, D. Moldovan, and F. M. Peeters, J. Appl. Phys. **118**, 154308 (2015).
[40] H. Ajiki and T. Ando, J. Phys. Soc. Jpn. **65**, 505 (1996).
[41] T. Ando, T. Nakanishi, and R. Saito, J. Phys. Soc. Jpn. **67**, 2857 (1998).
[42] J. L. Garcia-Pomar, A. Cortijo, and M. Nieto-Vesperinas, Phys. Rev. Lett. **100**, 236801 (2008).
[43] A. Rycerz, J. Tworzydło, and C. W. J. Beenakker, Nat. Phys. **3**, 172 (2007).
[44] D. Xiao, W. Yao, and Q. Niu, Phys. Rev. Lett. **99**, 236809 (2007).
[45] R. V. Gorbachev, J. C. W. Song, G. L. Yu, A. V. Kretinin, F. Withers, Y. Cao, A. Mishchenko, I. V. Grigorieva, K. S. Novoselov, L. S. Levitov *et al.*, Science **346**, 448 (2014).
[46] Y. Jiang, T. Low, K. Chang, M. I. Katsnelson, and F. Guinea, Phys. Rev. Lett. **110**, 046601 (2013).
[47] M. Settnes, S. R. Power, M. Brandbyge, and A.-P. Jauho, Phys. Rev. Lett. **117**, 276801 (2016).
[48] J. N. L. Connor and D. Farrelly, J. Chem. Phys. **75**, 2831 (1981).
[49] S. Yu. Dobrokhotov, G. N. Makrakis, V. E. Nazaikinskii, and T. Ya. Tudorovskii, Theor. Math. Phys. **177**, 1579 (2014).
[50] T. Pearcey, Philos. Mag. **37**, 311 (1946).
[51] J. N. L. Connor and D. Farrelly, Chem. Phys. Lett. **81**, 306 (1981).
[52] J. N. L. Connor and P. R. Curtis, J. Phys. A: Math. Gen. **15**, 1179 (1982).
[53] C. W. Groth, M. Wimmer, A. R. Akhmerov, and X. Waintal, New J. Phys. **16**, 063065 (2014).
[54] C. W. J. Beenakker and H. van Houten, Phys. Rev. Lett. **63**, 1857 (1989).
[55] S. P. Milovanović, M. R. Masir, and F. M. Peeters, J. Appl. Phys **113**, 193701 (2013).
[56] L. V. Berlyand and S. Yu. Dobrokhotov, Dokl. Akad. Nauk SSSR **296**, 80 (1987) [Sov. Phys. Dokl. **32**, 714 (1987)].
[57] V. V. Belov, S. Yu. Dobrokhotov, and T. Ya. Tudorovskiy, J. Eng. Math. **55**, 183 (2006).
[58] See Supplemental Material at http://link.aps.org/supplemental/10.1103/PhysRevB.96.045305 for additional simulation results, as well as details on the numerical implementation and additional derivations.
[59] L. Brey and H. A. Fertig, Phys. Rev. B **73**, 235411 (2006).
[60] T. O. Wehling, K. S. Novoselov, S. V. Morozov, E. E. Vdovin, M. I. Katsnelson, A. K. Geim, and A. I. Lichtenstein, Nano Lett. **8**, 173 (2008).
[61] R. R. Nair, I.-L. Tsai, M. Sepioni, O. Lehtinen, J. Keinonen, A. V. Krasheninnikov, A. H. Castro Neto, M. I. Katsnelson, A. K. Geim, and I. V. Grigorieva, Nat. Commun. **4**, 2010 (2013).
[62] C. Lee, J. Kim, S. Kim, Y. J. Chang, K. S. Kim, B. Hong, and E. J. Choi, Sci. Rep. **6**, 21311 (2016).
[63] A. Khademi, E. Sajadi, P. Dosanjh, D. A. Bonn, J. A. Folk, A. Stöhr, U. Starke, and S. Forti, Phys. Rev. B **94**, 201405(R) (2016).
[64] V. T. Phong and J. F. Kong, arXiv:1610.00201.
[65] M. Z. Hasan and C. L. Kane, Rev. Mod. Phys. **82**, 3045 (2010).
[66] X.-L. Qi and S.-C. Zhang, Rev. Mod. Phys. **83**, 1057 (2011).
[67] R. D. Y. Hills, A. Kusmartseva, and F. V. Kusmartsev, Phys. Rev. B **95**, 214103 (2017).